Microsystem Technologies 7 (2001) 63–70 © Springer-Verlag 2001

A MUMPs angular-position and angular-speed sensor with off-chip wireless transmission

W. Sun, W. J. Li, Y. Xu

Abstract A novel surface-micromachined non-contact high-angular-speed sensor with total surface area under 4 mm^2 was developed using the multi-user MEMS processes (MUMPs), and was integrated with a commercial RF transmitter with carrier frequency of 433 MHz for wireless signal detection. This piezoresistive sensing system is capable of wirelessly measuring rotation speeds with sensitivity of ~2 Hz/rpm/V using 5 V input in the 100–6000 rpm rotation range. Further experimental analyses showed that a sensor designed with a 13 μg seismic mass has high enough sensitivity to detect angular position of a rotating disk if the disk rotation axis is tilted away from the vertical direction. Experimental results from simultaneous detection of angular position and average angular speed for the sensor are reported in this paper.

1 Introduction

Tachometers have been widely used to measure angular speeds of rotating objects. In general, contact mechanical-based tachometers, although capable of giving measurements conveniently, are less accurate than AC or DC electromagnetic-based tachometers. Nevertheless, as discussed by Nachtigal (1990) and Haslam et al. (1993), each type has its own advantages and shortcomings depending on the applications. Optical tachometers are also available to give relatively accurate readings with a wide rpm range. An example of this optical measurement method is given by Spooncer et al. (1991). However, Kwa and Wolffenbuttel (1991) pointed out that some optical sensors are quite sensitive to background light and contamination.

Recently, many new rotation-sensing devices were developed based on different principles. Watanabe and Kim (1994) measured rotation speed from magnetized axes, Powell and Meydan (1996) used magnetic sensors based on Faraday induction to measure rotation rate, and Fabian and Brasseur (1997) developed a capacitive sensor for angular motion detection. These techniques, however, impose restrictions on the material properties or geometry of the rotational components to be measured, and they also limit the effective measurable rotation speed. In addition, all these sensors must be accompanied with a stationary reference, which is externally mounted to the systems' housing for proper operation.

Many micro motion sensors have also been fabricated recently which can be used for rotation sensing. Söderkvist (1990), Madni et al. (1996), and Voss et al. (1997) used piezoresistive, piezoelectric, and capacitive principles, respectively, for angular rate sensing. Nonetheless, the existing sensors are designed mainly for low rotation speeds (i.e., <1000 rpm) and acceleration measurements.

We have previously developed a MEMS high-speed rotation sensor with no external mounted reference and it was packaged with a commercial wireless-transmission system for signal detection. Results of this work can be obtained from Sun et al. (1999, 2000). This piezoresistive sensor is capable of wirelessly measuring rotation speeds with sensitivity of ~2 Hz/rpm/V using 5 V input in the 100–6000 rpm rotation range. To the best of our knowledge, no one has reported successful integration of high-speed rotation sensors built using the MCNC (renamed to CRONOS Integrated Microsystems Inc.) MUMPs commercial foundry service with wireless transmitted output before our work.

In the current work, we have tested several structural and seismic mass designs for the above sensor to observe if the sensing system has enough sensitivity to detect gravitational effect if the system is rotated about an axis parallel to the ground. We have found that, for certain seismic mass and structural design combinations, the sensing system is capable of detecting gravitational force, and hence, can be used simultaneously as a angular-position sensor. It is well known that, for surface-micromachined devices, gravity force is less important when compared to surface forces. However, for our sensor design and high-speed measurement range, centrifugal force will overcome surface forces, and hence, making the sensor angular-position sensitive. The result from the currently work is reported in this paper.

2 MUMPs fabricated rotation sensor

Concept and design

The concept for measuring rotation speed of a spinning body using embedded micro-sensors is illustrated in

Received: 5 May 2000/Accepted: 31 August 2000

W. Sun, W. J. Li (✉), Y. Xu
Department of Automation and Computer-Aided Engineering,
The Chinese University of Hong Kong,
MMW 425, Shatin, N.T.,
Hong Kong
E-mail: wen@acae.cuhk.edu.hk

This work was funded by the Chinese University of Hong Kong Research Direct Grant (2050173) and the Information Technology Entrepreneurs Program Grant (6900916).

Fig. 1. A three dimensional illustration of the developed MCNC sensor is shown in Fig. 2. Details of the MCNC layers and post-fabrication processes used were reported by Sun et al. (1999). Scanning electron microscope (SEM) picture of a pair of the surface-micromachined sensors is shown in Fig. 3. The mass platforms are sacrificially released and are curved due to residual stresses between different thin film layers in this case. Three MUMPs thin film layers which make up the platforms are apparent in this picture: Poly 1, Poly 2, and Au. A reference sensor that was not sacrificially released is shown in Fig. 4. The reference sensor can be used for temperature dependence adjustment of the sensing system eventually.

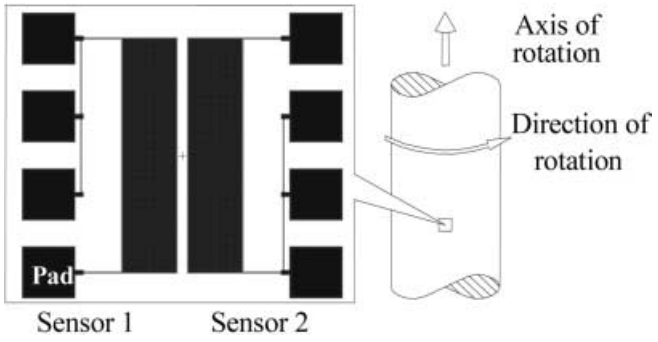

Fig. 1. Conceptual drawing of micro sensors embedded in a rotating structure to measure rotation (not to scale)

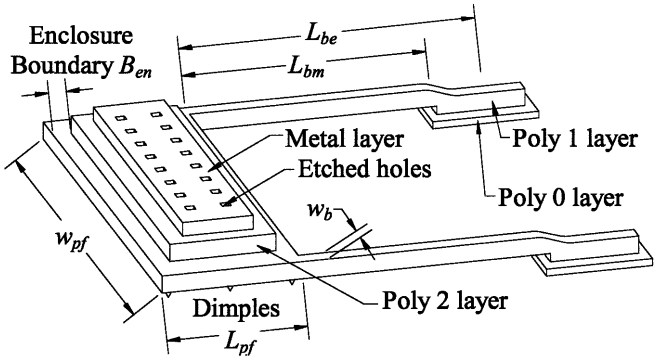

Fig. 2. Three-dimensional drawing of a surface-micromachined rotation sensor using polysilicon as cantilever beams supporting a multi-layered mass platform

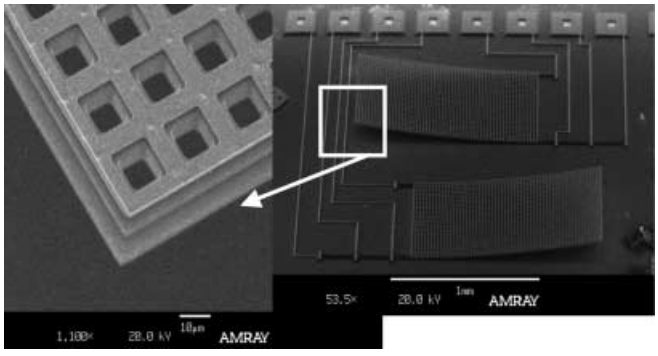

Fig. 3. SEM picture of a pair of fabricated sensors. The curvature of the mass plate is due to residual stress between different layers of materials making up the plate. The MUMPs layers shown are Poly 1, Poly 2, and Au

Theoretical analysis

As shown in Fig. 5, a set containing two identical sensors in opposite directions is oriented so that the axes of the cantilevered beams are perpendicular to the axis of rotation. As will be discussed later, a set of two sensors can be used to measure the angular acceleration of the rotating element.

If no linear motion exists along the rotation axis then lateral deflection of the beams, or transverse stress, can be neglected. Excluding the substrate, a MCNC fabricated sensor is less than 5.1 μm thick (platform) and weighs about 3–15 μg (theoretical value based on the density and geometric dimensions of the materials). As shown in Fig. 5, the initial moment arm from the centroid c to the fixed end **F** is a constant. When centrifugal force is induced on the seismic mass by an angular velocity (ω) or acceleration (α), the length of this moment arm will change. The vertical load $P = m \cdot r \cdot \omega^2$ induced by rotation and the axial load $N = m \cdot r \cdot \alpha$ caused by angular acceleration (r is the distance from the axis of rotation to the neutral axis of the cantilever) both act on the centroid c of the platform. The distance e_c is a constant depending on the number of polysilicon layers. It is measured from the

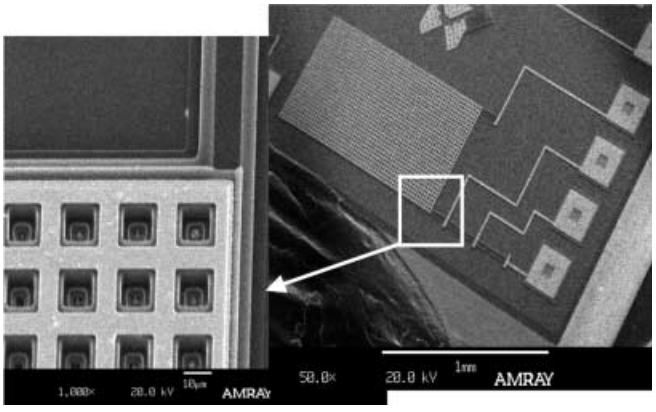

Fig. 4. SEM picture of a reference sensor. MUMPs layers shown in the SEM include Poly 0, Poly 1, Poly 2, and Au

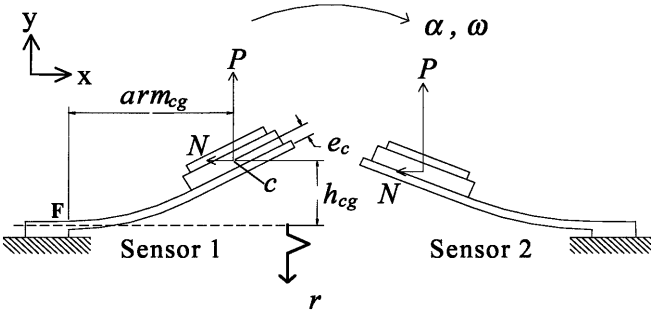

Fig. 5. This illustration shows a pair of rotation sensors. The design parameters are also shown in this figure

centroid of the platform to the neutral axis of the beam. The maximum strain on the cantilever beams occurs at **F**, the fixed end of the beams. From Fan et al. (1988), the maximum allowable strain of polysilicon is about 1.7%. At $t > 0$ s, the platform will be raised by a distance h_{cg} due to centrifugal force. Consequently, the beams will be under stress and deformed in a curved shape. The beams will also undergo slight elongation or shortening depending on the combined effect of P and N. The moment arm measured from the fixed end **F** to the centroid will also be shifted from initial distance to arm_{cg}.

The governing differential equation for the bending beam is shown in (1) below. The moment and stress equations are shown in (2) and (3), respectively.

$$EI\frac{d^2y_i}{dx_i^2} + P\cdot x \pm N\cdot y - M_i = 0, \quad i = 1,2 \tag{1}$$

$$M_i = P\cdot \text{arm}_{cg} \pm N\cdot h_{cg}, \quad i = 1,2 \tag{2}$$

$$\sigma_i = -\left(\frac{M_i\cdot t\cdot (f-1)}{6\cdot I_w} \pm N/A_{bm}\right), \quad i = 1,2 \tag{3}$$

The index i denotes sensors 1 and 2 in Fig. 5. In (3) I_w is the moment of inertia of the cross-section area about the neutral axis. $A_{bm} = t_{bm}\cdot(2\cdot w_{bm})$ is the total cross-section area of the two beams, t is the beam thickness, and f is the wedge factor equals to the ratio of beam-center-width to beam-bottom-width. The neutral axis is not at $t_{bm}/2$ for MCNC fabricated beams due to the fabrication process which causes the beams to have a trapezoidal cross-section. (2) is obtained by summing the moments about any arbitrary point (x_i, y_i) along the beam i. Analytical solutions of (1) can be readily obtained from symbolic mathematical packages (e.g., Mathematica) for a given set of values of r, ω and α. For transient calculations, the results of (1) can be used to obtain arm_{cg} and h_{cg} at a given time, which can then be used in (2) to obtain a more accurate solution.

The deflection or elongation of the beams causes a change of resistance of the polysilicon, which can be converted into a measurable change of voltage by connecting the sensors in a Wheatstone-bridge configuration. The change of resistance due to beam elongation can be expressed as a function of gauge factor G. This is shown in (4):

$$\frac{\Delta R_l}{R} = \frac{G}{L_{bm}}\cdot\int_0^{L_{bm}}\frac{\sigma_i}{E}dx \tag{4}$$

where R is the total resistance of the sensor and for polysilicon is typically about $10\,\Omega/\square$, as given by Koester et al. (1996). σ_l is the longitudinal stress in (3), and σ_t is the transverse stress which can be neglected at steady-state conditions. When a steady-state rotational speed is achieved, the axial load N tends to zero. The two sensors will have the same deflection and change of resistance. However, when the angular acceleration α is >>0, such as during motor startup or under sudden change of speed, the transient response of Sensor 1 and Sensor 2 will be different due to the contribution from N. Hence, by monitoring the transient response of the sensors, the direction of acceleration can be determined. We have used the above theoretical analysis in designing the sensors to measure angular speeds up to 6000 rpm.

3 Experimental results

Wireless transmission circuit system

Commercial wireless transmitters and receivers, which can be eventually interfaced with our rotation sensors, were evaluated for signal transmission. Two basic configurations were evaluated. The first configuration maps the analog voltage output from the sensor into digital data before RF transmission by the transmitter. The volume of the entire transmitter circuitry, including the sensor, battery, and IC-packaged ADC, clock, and RF transmitter is about $1\times3\times3$ cm. When the ADC, clock, and RF transmitter die are used instead of the IC packaged chips the entire transmitter circuitry should be significantly smaller. The second type of transmission scheme maps the voltage from a sensor into frequency before the RF transmission. The overall volume of the IC-packaged chips for this scheme is only 1/3 the size of the previous method but a frequency counter must be used at the receiver end to decipher the original voltage information. We have adopted the second configuration at this time because it is simpler to build and has a good transmission performance experimentally. However, we have found that the TX2 transmitter (Radiometrix) works better than the HX2000 (RFM) for our sensors.

The configuration is implemented as shown in Fig. 6. The change of resistance across the bending beams is transduced into a change of differential voltage and then amplified by the AMP04 instrumentation amplifier, which has an adjustable gain between 1 and 1000. The amplified voltage is then converted into a frequency signal by an AD654 voltage to frequency converter. This stage is essential for the TX2 transmitter to provide stable signal transmission. The potentiometer at R_4 should be adjusted such that variation of bridge output is beyond the initial offset and within the linear region of AMP04 as well as bounded by the upper frequency limit of TX2 at around 28 kHz (carrier frequency of 433 MHz). The signal is

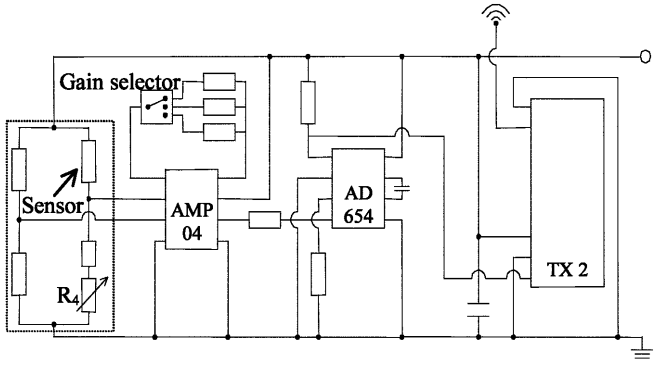

Fig. 6. Schematic drawing of the wireless transmission circuit system used to transmit the surface-micromachined sensor

detected wirelessly by the Radiometrix RX2 (not shown in the figure).

Angular-speed sensing

The conceptual drawing and a picture of the actual experimental setup to measure rotation speeds of a disk are shown in Fig. 7. In our design, the rotating disk is replaceable. The power supply and the wireless transmission system chips are placed within a small package, which was made by a CNC plastic injection machine, and then placed on the rotating disk.

The MCNC fabricated sensors were tested for piezoresistivity by using probes to lift the platforms while measuring changes in resistance across the beam-platform-beam connection (see Fig. 2). The variations of resistance versus deflection angle of the platform from the substrate for several sensor designs were tested and were shown to be non-linear but very consistent.

As predicted by theory, narrower beams give higher resistance change and are prone to structural failure at higher deflection angles. For instance, $14 \times 100\,\mu m$ beams will fail at $\sim 60^\circ$ while 20×200 and $30 \times 200\,\mu m$ beams will survive beyond deflections angles of $\sim 80^\circ$. The circuit shown in Fig. 6 was calibrated such that the frequency output of the AD654 is linear from 10–25 kHz with ~20% change of resistance in the Wheatstone bridge. The bridge output was connected via wirebonding to pads on a PCB that contains the signal transmission circuitry. Typical frequency output received by the RX2 receiver as the sensor is rotated is shown in Fig. 8. The response of the sensor (Fig. 8), is non-linear as predicted, since the supporting cantilevered beams underwent large deflections over the dynamic range tested.

To validate the signal received by the receiver is indeed rotation data, we have used (1)–(4) (if the electronic gains are know a priori) to model the received frequency in the wireless transmission circuit versus the rotation speed. However, (1) and (3) have assumed small and linear deflection in their formulation, hence cannot predict the frequency output accurately for the entire experimental dynamic range, since the sensor structures will undergo large and non-linear deflections at high speeds. Nevertheless, if $\Delta R/R$ from (4) is replaced with the experimental results from probe-lifting (Fig. 9), the pseudo-model predicts the experimental data closely. Hence, the received frequency can be concluded as rotation data from the

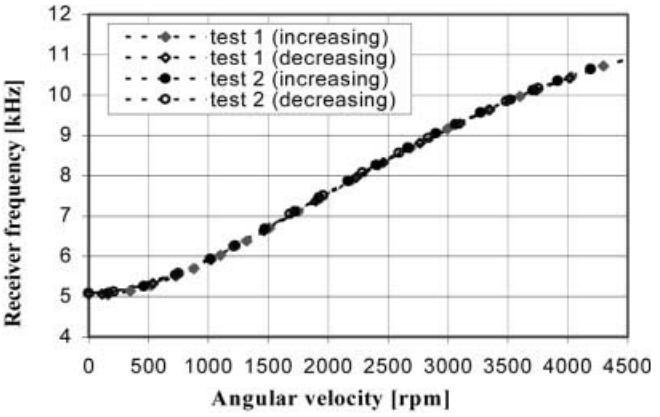

Fig. 8. Wireless transmitted data from a rotation sensor. The sensor has a $1200 \times 600\ \mu m^2$ platform supported by $20 \times 100\ \mu m^2$ beams, and was rotated on a 10 cm disk. Some sensors were tested up to 6000 rpm before beam failure

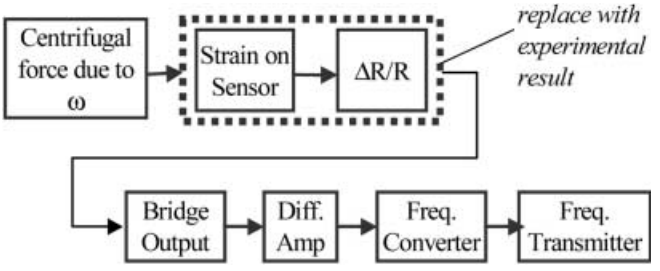

Fig. 9. Schematic transfer function diagram of the sensor output frequency versus input ω. In the pseudo-model, $\Delta R/R$ is replaced with probe-lifting experimental data

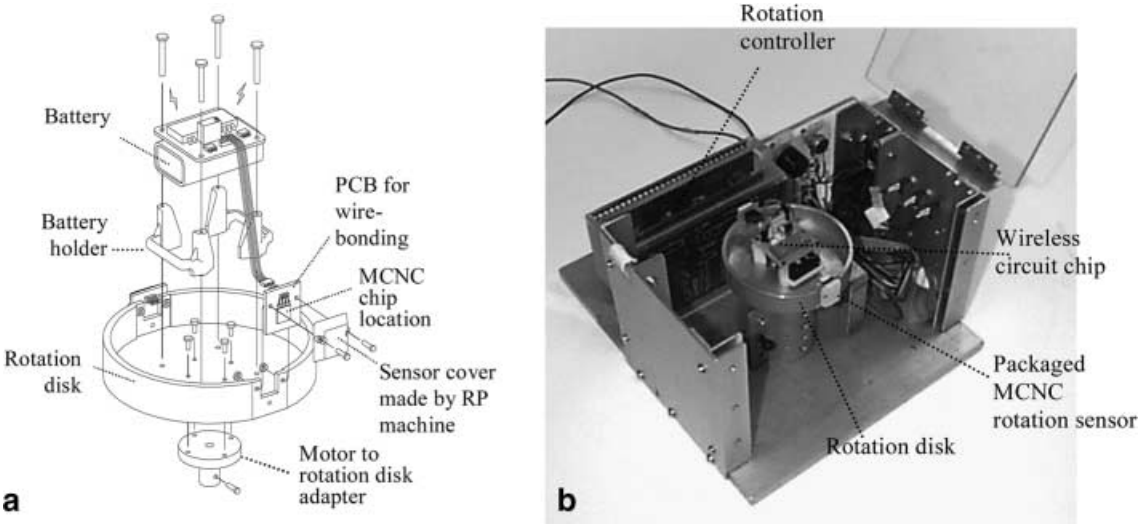

Fig. 7. **a** Conceptual drawing and **b** actual picture of the experimental rotating disk packaged with wireless rotation MEMS sensor

micro sensor. The comparison between the experimental results, the linear-deflection theory, and the pseudo-model is shown in Fig. 10.

The sensors were also subjected to vibration and temperature tests, and the results were presented by Sun et al. (2000).

Angular-position sensing

We have oriented the experimental setup (Fig. 7) at different angles relative to the *Z*-axis (axis perpendicular to the horizontal plane) as shown in Fig. 11 and tested the effects of gravity on the sensor signal output. The wireless signal transmission system was found to have enough sensitivity to measure fluctuations in sensor output due to gravity.

For simplicity, if the aerodynamic forces are neglected, the total radial force F_r acting on the seismic mass as it rotates around a disk of radius r is:

$$F_r = m \cdot (r\omega^2 - g \sin\theta \sin\phi) \tag{5}$$

where m is the mass of the platform. This equation indicates that the gravitational effect can be neglected as long as r or ω is sufficiently large. However, if m is large enough, a sensing system may be able to detect F_r as a function of θ and ϕ, for some bounded values of r and ω. A plot of the ratio of gravitation force F_g and centrifugal force F_c on any given m is shown in Fig. 12 for several disk radii (assuming $\theta = 90^\circ$ and $\phi = 180^\circ$). For our sensing system, we are able to detect an F_g/F_c ratio of about 0.2% at 3000 rpm for a 5 cm radius disk.

A Turbo-C program was written to simultaneously acquire rotation speed signal from the optical encoder and frequency signal that is proportional to the angular-position and velocity from the receiver. A two-channel programmable I/O device (8255 card) was used under the Windows 95 environment, which also serves as an interface between the computer and the external 16-bit counter that is made of four cascaded 4-bit counters. The number of counting cycles is predefined as n at the beginning of the program. It terminates at $t = t_f$, and the total time taken for counting n number of cycles is T_t, which is approximated by summing up all individual periods from T_1 to T_n. The maximum number of counts of the external 16-bit counter is $2^{16} = 65536$, and the 8255 clock speed is 2.073 MHz. Hence, the lowest theoretical measurable frequency by the computer is therefore $2.073 \times 10^6/65536 \approx 31.6$ Hz. This is adequate for our current use because the lowest received RF signal from the wireless transmitter is 1 kHz and the lowest rotation speed tested is typically greater than 50 rpm (at 500 slots per revolution, this corresponds to ~417 Hz). Depending on the requirements, this frequency can be further lowered or raised if necessary, by adding more cascade counters or utilizing an external oscillator at a known higher frequency, respectively. An illustration describing how the variations in frequencies are counted is shown in Fig. 13.

We have tested the wireless rotation sensing system on a 5 cm disk that was tilted at different θ. The results are presented below.

As seen in Fig. 14, the peak-to-peak variation at 300 rpm and 0° tilt is less than 3 Hz (frequency signal received by the receiver), which when compared to the nominal frequency around 1.06 kHz, is less than 0.3% and considered negligible.

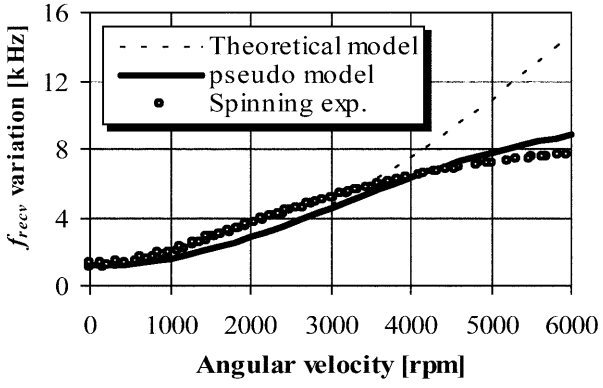

Fig. 10. Comparison of experimental, theory, and theory plus lifting-experiment results. The theory under-predicts sensor output at lower rpms possibly due to two factors: (1) piezoresistive change of the mass platform and (2) aerodynamic lifting of the mass platform

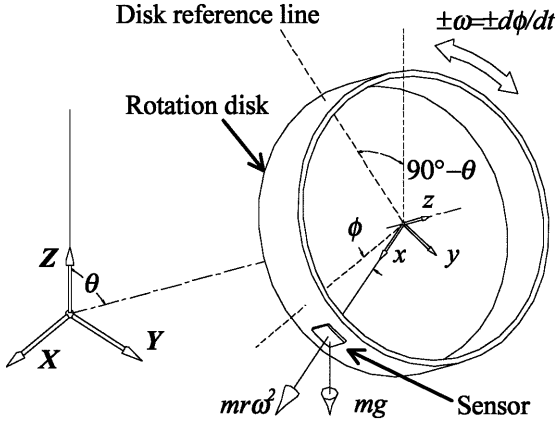

Fig. 11. Conceptual drawing of the rotation setup showing definitions of θ, ϕ, and forces acting on the sensor

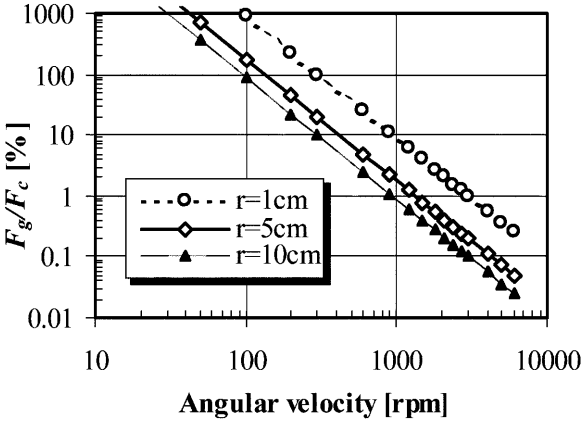

Fig. 12. Variation of force in radial direction with respect to change in sensor angular position and tilt angle at 500 rpm

However, when the disk is tilted at 90°, a clear sinusoidal wave appears and the fluctuating amplitude is ~30 Hz (Fig. 15). This data was compared to the theoretical dependence of output on ϕ, as give by (5), in the same figure, and shows that the data is indeed due to the dependence of the sensor output on gravity. Hence, angular position of the sensor on the disk can be obtained if the sampling frequency is sufficiently high and the output signal is calibrated. However, as shown in Fig. 15, the sensor output is at 323.4 rpm, which differs from the optical encoder output of 300 rpm. We have found that the difference is due to the mis-calibration of the optical encoder output, which illustrates an advantage of this gravity-dependent angular speed and position sensor: as along as the sensing system is able to give full peak-to-peak cyclical measurement, it does not need to be calibrated for receiver frequency drift. That is, ω and ϕ can be obtained from counting the cycles per unit time and measuring the instantaneous output amplitude, respectively.

The power spectrum density (PSD) of the output signals can also be obtained to find ω. Matlab was used to analyze our experimental data. The PSD for 300 rpm at 0° tilt signal is shown in Fig. 16. Theoretically, if a sensor rotating at 300 rpm has its output dependent on gravity, then the output signal should have spectrum peak at $f = \omega/60 = 5$ Hz (the mass will undergo 1 cyclic vibration for every $\phi = 360°$). From Fig. 16, however, the dominant peaks are below 0.2 Hz, and most likely are due to $1/f$ noise effect. The PSD of the same sensor tilted at 90° is shown in Fig. 17, which visibly shows a peak at 5.39 Hz. The error is possibly due to the mis-calibration of the optical encoder, as discussed before. Nevertheless, this indicates that the dominant spectrum signal is due to dependence of the sensor on ϕ. This also indicates that obtaining the PSD could be an alternative method to read the rotation speed.

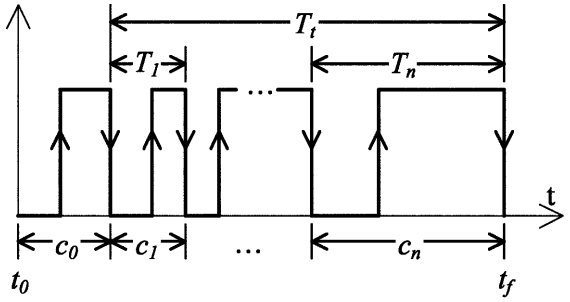

Fig. 13. Illustration showing how the variations in frequencies are counted

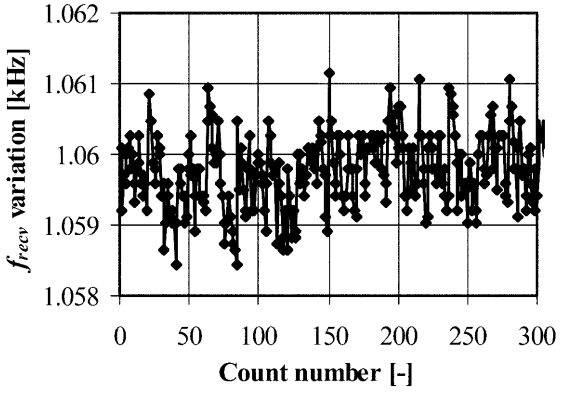

Fig. 14. Receiver frequency variation of the sensor at 300 rpm with 0° tilt

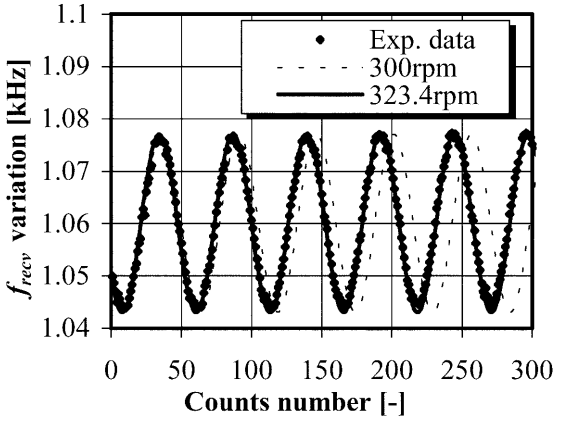

Fig. 15. Receiver frequency variation of the sensor at 300 rpm with 90° tilt. The experimental data is also compared to modeled data

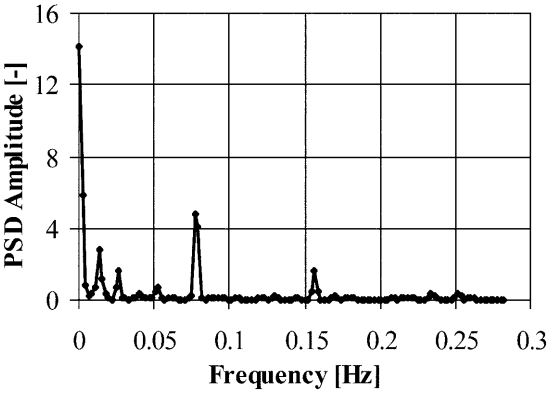

Fig. 16. FFT spectrum showing peaks for a sensor tilted at 0° rotating at 300 rpm

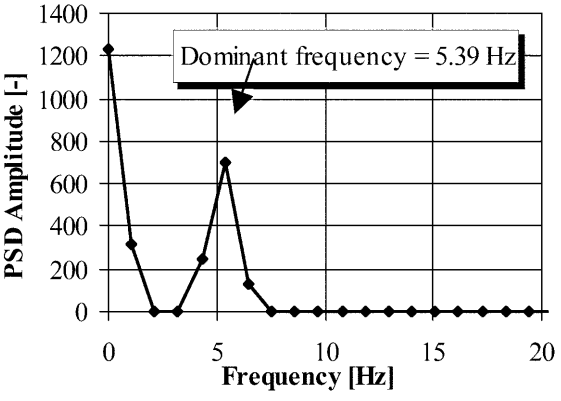

Fig. 17. FFT spectrum showing peak at 5.39 Hz for a sensor tilted at 90° rotating at 300 rpm

At rotation speed of 3000 rpm with 90° tilt, the receiver frequency variation is shown in Fig. 18. The sinusoidal waveform is not as obvious compared to that from 300 rpm. However, as shown in Fig. 19, the PSD peaks at 53.8 Hz, corresponding 3228 rpm.

Experimental data were also obtained for the sensing system tilted at different θ and rotated at different angular speeds. Amplitude of the output signal variation is confirmed to be less at higher rotation speeds for any given tilt angle θ. The results of $\omega = 300$ and 1200 rpm are shown in Fig. 20. However, if the output is time averaged, the sensor output is independent of θ as shown in Fig. 21. Hence, the sensing system can also be used to sense ω, irrespective of θ.

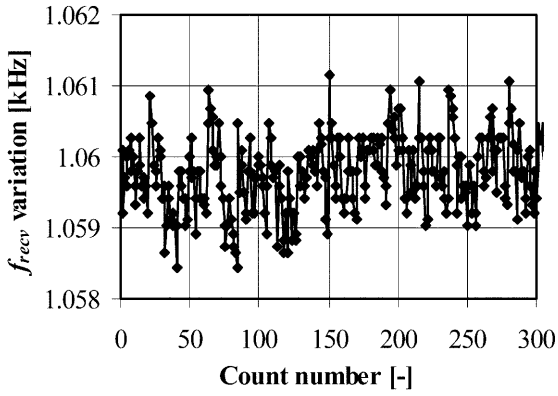

Fig. 18. Time sequence signal of sensor rotating at 3000 rpm with 90° tilt

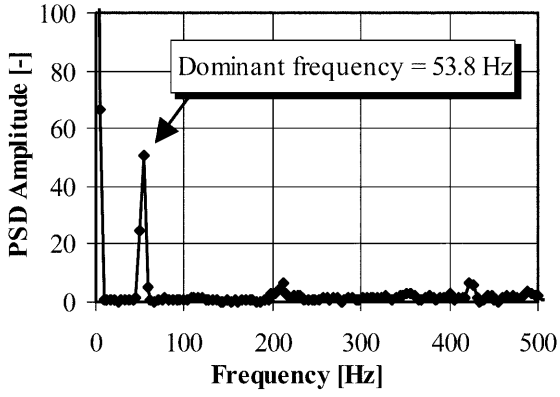

Fig. 19. PSD of sensor rotation at 3000 rpm with 90° tilt

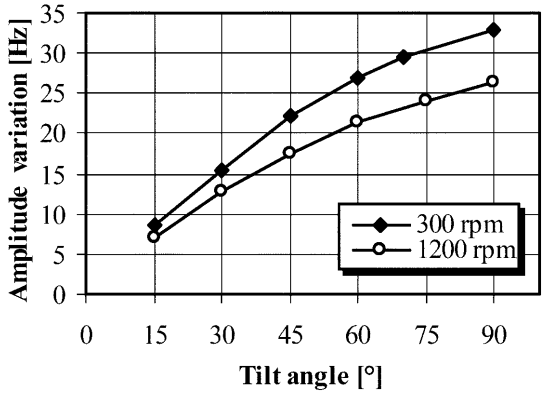

Fig. 20. Variation of peak-to-peak amplitude of the receiver frequency at 300 and 1200 rpm at different tilting angles

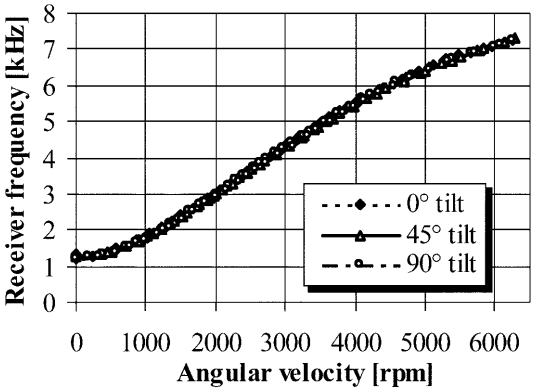

Fig. 21. Orientation has insignificant effect on the overall trend of the receiver frequency response if the signal is averaged over time

4 Conclusion

The design of a novel surface-micromachined rotation sensor for high-angular-speed detection is presented. It is designed to detect the angular velocity of a rotating element by measuring the resistance change due to stress induced by centrifugal force on the seismic mass using piezoresistive effects. The designed sensors were fabricated using the MUMPs-29 run. Several wireless transmission schemes for the rotation sensing system were evaluated, and the Radiometrix TX2 transmission chip was eventually used for our experiments. Experimental results showed a 13 μg platform proof-mass could be used to detect rotation speeds of 100–6000 rpm if appropriate structural designs are implemented. The sensing system is also capable of detecting angular-position wirelessly at lower rpms for a 5 cm disk. We will further improve the sensing system by interfacing it with low-power wireless circuits and test the feasibility of using a pair of co-located structures for angular acceleration detection.

References

Fabian T; Brasseur G (1997) A robust capacitive angular speed sensor. IEEE IMTC '97, 2: 1267–1272

Fan LS; Tai YC; Muller RS (1988) Integrated movable micromechanical structures for sensors and actuators. IEEE Trans Elec Dev 35: 724–730

Haslam JA; Summers GR; Williams D (1993) Engineering Instrumentation and Control, London, Edward-Arnold, p 133

Koester DA; Mahadevan R; Hardy B; Markus KW (1996) SmartMUMPs Design Handbook, Rev. 4.0, MEMS Technology Applications Center

Kwa TA; Wolffenbuttel RF (1991) An integrated high-resolution optical angular displacement sensor. IEEE Transducers '91, 368–371

Madni AM; Wan LA; Hammons S (1996) A microelectromechanical quartz rotational rate sensor for inertial applications. IEEE Aeros App Conf 2: 315–332

Nachtigal CL (1990) Instrumentation and Control – Fundamentals and Applications, New York, Chichester, Wiley, p 370
Powell A; Meydan T (1996) Optimisation of magnetic speed sensors. IEEE Trans Mag '96, 32: 4977–4999
Söderkvist J (1990) Piezoelectric beams and angular rate sensors. IEEE Proc on the 44th Annual Symposium On Frequency Control 406–415
Spooncer RC; Nicholson AS; Oliver MR (1991) An optical tachometer with optical fibre links. IEE Colloq IREM 1–3
Sun W; Mei T; Ho W-T; Li W (1999) A MEMS high-speed rotation measurement system with MCNC fabricated motion and reference sensors using wireless transmission. IEEE International Conference on Multisensor Fusion and Integration for Intelligent Systems, Taipei 226–231
Sun W; Ho W-T; Li W; Mai JD; Mei T (2000) A foundry fabricated high-speed rotation sensor using off-chip RF wireless signal transmission. IEEE MEMS 358–363
Voss R; Bauer K; Ficker W; Gleissner T; Kupke W; Rose M; Sassen S; Schalk J; Seidel H; Stenzel E (1997) Silicon angular rate sensor for automotive applications with piezoelectric drive and piezoresistive read-out. IEEE Transducers 2: 879–882
Watanabe K; Kim C (1994) Non-contact revolution measurement by the magnetic field intensity from axes. IEEE IMTC '94, 2: 605–608